Effects of Transmitter Symbol Clock Jitter Upon Ground Receiver Performance

Meera Srinivasan*, Andre Tkacenko*, Mark Lyubarev†, and Polly Estabrook*

In this article we characterize the effect of transmitter clock jitter upon receiver symbol synchronization performance. Using a sinusoidal model for the timing jitter, we evaluate the bit error rate (BER) degradation and cycle slip probabilities of receivers via analysis as well as simulation for uncoded offset quadrature-phase-shift-keying (OQPSK). We evaluate performance for two different symbol synchronization loops: the modified data transition tracking loop (M-DTTL) and the Gardner loop. The results are parameterized in terms of the timing jitter parameters (peak frequency jitter, time interval error, and cycle-to-cycle jitter) as well as symbol tracking loop parameters (loop damping factor, loop bandwidth). We present analytical expressions for BER degradation in the presence of sinusoidal timing jitter and compare results with those obtained via simulation, as well as past hardware tests of receivers. These results show that for both types of symbol synchronizers, peak BER degradation decreases as the loop damping factor increases, and that for underdamped tracking loops, the BER degradation peaks when the normalized jitter rate is approximately the same as the natural frequency of the loop transfer function. Simulated cycle-slip rates are also presented, showing the effects of varying loop bandwidths and damping factors. Finally, we illustrate how BER degradation can be characterized in terms of jitter time interval error and cycle-to-cycle jitter, providing predictive capabilities for receiver performance and guidelines for the specification of transmitter clock requirements.

I. Introduction

In space communications the transmit symbol clock and receiver clock are asynchronous; hence the phase and frequency offset between the clocks must be tracked and compensated

*Communication Architectures and Research Section

†formerly of the Communication Architectures and Research Section

The research described in this publication was carried out by the Jet Propulsion Laboratory, California Institute of Technology, under a contract with the National Aeronautics and Space Administration.

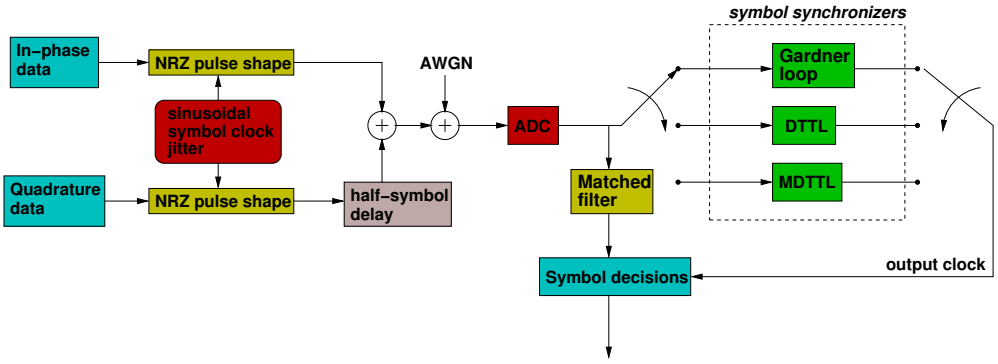

Figure 1. Baseband equivalent model of receiver system.

for in order to avoid significant losses in receiver performance. By utilizing modern error correction codes such as low density parity check (LDPC) codes, ground receivers operate at low signal-to-noise ratios (SNR), rendering them susceptible to the effects of symbol timing jitter, which causes bit error rate (BER) degradation as well as potential cycle slips in tracking the symbol clock. In particular, symbol slips are catastrophic events that cause the loss of whole data frames. The ability to track the clock offset depends upon the characteristics of the receiver tracking loop as well as the severity and nature of the transmit clock jitter. Certain commercial receivers that are being considered for use in NASA's ground receiver infrastructure have limited configurability, and laboratory measurements show BER degradation and increased cycle slip rates in the presence of timing jitter [1]. Furthermore, NASA's Space Network User's Guide (SNUG) [2] contains requirements for satellite transmit clock specifications in the form of a symbol timing jitter mask. Our goal is to develop predictive analytical tools in order to improve the formulation of such jitter specifications. In this article we evaluate receiver performance in terms of uncoded bit error rate (BER) degradation as well as probability of cycle slips in the presence of sinusoidal transmitter clock jitter.

We will first describe the system model, including the signal model, receiver tracking loop structure, and the sinusoidal clock jitter model. We then describe analysis and simulation results showing the impact on BER degradation, followed by cycle slip probability results. We conclude by comparing our results with the SNUG jitter mask.

II. System Model

A. Signal Model

Figure 1 depicts a block diagram of the baseband system model. An offset quadrature phase shift keying (OQPSK) signal is transmitted under the assumption of a non-ideal transmit symbol clock with sinusoidal symbol jitter. After thermal noise is added to the transmitted signal, the complex baseband received input to the ADC is given by

$$\tilde{r}(t) = \sqrt{2P}\left((d_I(t-\tau(t)) + jd_Q(t-T/2-\tau(t))\right) + n(t)$$

where P is the average signal power, T is the symbol duration, and $\tilde{n}(t)$ is complex additive white Gaussian noise (AWGN). The OQPSK in-phase and quadrature data modulation waveforms $d_I(t)$ and $d_Q(t)$ are given by

$$d_I(t) = \sum_{l=-\infty}^{\infty} d_l^{(I)} p(t - lT)\,,\; d_Q(t) = \sum_{l=-\infty}^{\infty} d_l^{(Q)} p(t - lT)$$

where the in-phase and quadrature data bits $d_l^{(I)}$ and $d_l^{(Q)}$ take on values ± 1 with equal probability and $p(t)$ is a rectangular non-return-to-zero (NRZ) pulse:

$$p(t) = \begin{cases} 1\,, & 0 \le t < T \\ 0\,, & \text{otherwise} \end{cases}$$

The received symbol timing offset $\tau(t)$ is modeled as the sum of a fixed delay τ_0 and a sinusoidal transmit clock jitter, i.e.,

$$\tau(t) = \tau_0 + \frac{1}{2\pi R_d} \frac{\Delta F_{PJ}}{F_{JR}} \sin(2\pi F_{JR} t + \phi)$$

Here, R_d is the symbol rate, ΔF_{PJ} is the peak jitter value, F_{JR} is the jitter rate value, and ϕ is an arbitrary phase offet. We consider three measures of jitter degradation: time interval error (TIE), frequency jitter (FJ), and cycle-to-cycle jitter (CCJ). For the sinusoidal jitter model, these measures are given by the following quantities:

$$\begin{aligned} \text{TIE} &= \frac{1}{2\pi} \frac{\Delta F_{PJ}}{F_{JR}} \\ \text{FJ} &= \Delta F_{PJ} \\ \text{CCJ} &= 2\pi F_{JR} \Delta F_{PJ} \end{aligned}$$

The time interval error is the time deviation of the clock edge from its ideal reference point, expressed as a percentage of the symbol interval length. Frequency jitter is the difference between the desired clock frequency and the actual clock frequency, and is expressed as a percentage of the symbol rate. Cycle-to-cycle jitter is the difference in clock frequency between any two adjacent cycles, and is expressed as a percentage of the symbol rate squared. In general, jitter may have stochastic as well as deterministic components. We only analyze deterministic, single-tone sinusoidal jitter here, although some simulation results are presented for multi-tone jitter.

B. Symbol Tracking Loop Model

The symbol timing recovery loop estimates the received symbol timing offset $\tau(t)$ and uses the estimate in order to determine which samples of the match-filtered signal output should be used as soft-symbol decision statistics. We initially consider three types of 2nd order symbol tracking loops in this article. The Data Transition Tracking Loop (DTTL), shown in Figure 2, is used in the DSN's Block V Receiver. It requires phase coherence prior to symbol tracking operation, and utilizes input from either the in-phase or quadrature stream of baseband samples. We also consider the two armed version of the

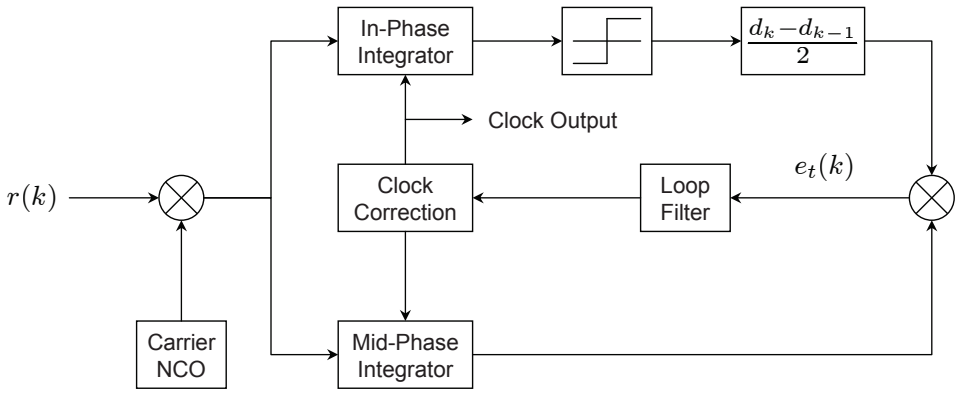

Figure 2. Data transition tracking loop block diagram.

DTTL, or modified DTTL (M-DTTL) (shown in Figure 3), in which both in-phase and quadrature data are used without requiring phase coherence. Both the DTTL and M-DTTL perform well for rectangular NRZ pulses, but suffer when used for pulse-shaped modulations such as square-root-raised-cosine (SRRC) signals. A more general type of symbol synchronizer is the Gardner loop, shown in Figure 4. The Gardner loop is also a noncoherent symbol synchronizer that may be implemented prior to carrier phase tracking; furthermore, it performs well for more general pulse shapes [3]. For purposes of BER degradation analysis, the conventional single-armed DTTL is used. In the Monte Carlo simulations, however, all three types of symbol tracking loops were tested.

In order to analyze this loop and design the loop filter, we examine the digital baseband equivalent loop diagram shown in Figure 5 described by the loop equation

$$\widehat{\tau}(k) = A\left(\tau(k-L) - \hat{\tau}(k-L)\right) * f(k) \tag{1}$$

The quantity $\widehat{\tau}(k)$ is the estimate of the timing offset τ at time k, A is the loop gain factor, and L is the bulk delay through the loop. The loop filter $f(k)$ is a second order filter with digital transfer function

$$F(z) = \frac{\alpha(1-z^{-1}) + \beta}{(1-z^{-1})^2} \tag{2}$$

where α and β are loop coefficients that are designed to obtain the desired response and loop bandwidth. The loop bandwidth is calculated as

$$B_l = \frac{1}{2}\int_{-1/2T_u}^{1/2T_u} \left|H\left(e^{j2\pi f T_u}\right)\right|^2 df \tag{3}$$

where T_u is the loop update time and $H(f) = H(z)|_{z=e^{j2\pi f T_u}}$ is the closed loop transfer function, which may be obtained from Equation (1) as

$$H(z) = \frac{AKF(z)}{z^L + AKF(z)} \tag{4}$$

Here, A is the amplitude of the the input signal, L is the bulk delay through the loop in units of update time, and $K = G_{pd}G_{nco}$ is the product of the phase discriminator gain and

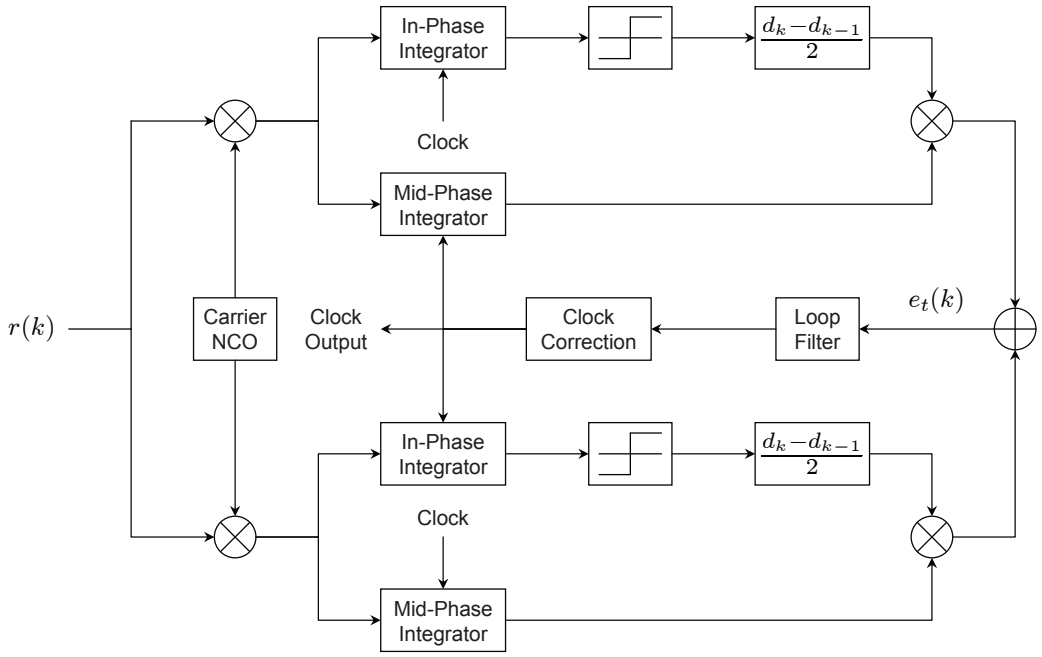

Figure 3. Modified data transition tracking loop block diagram (noncoherent version).

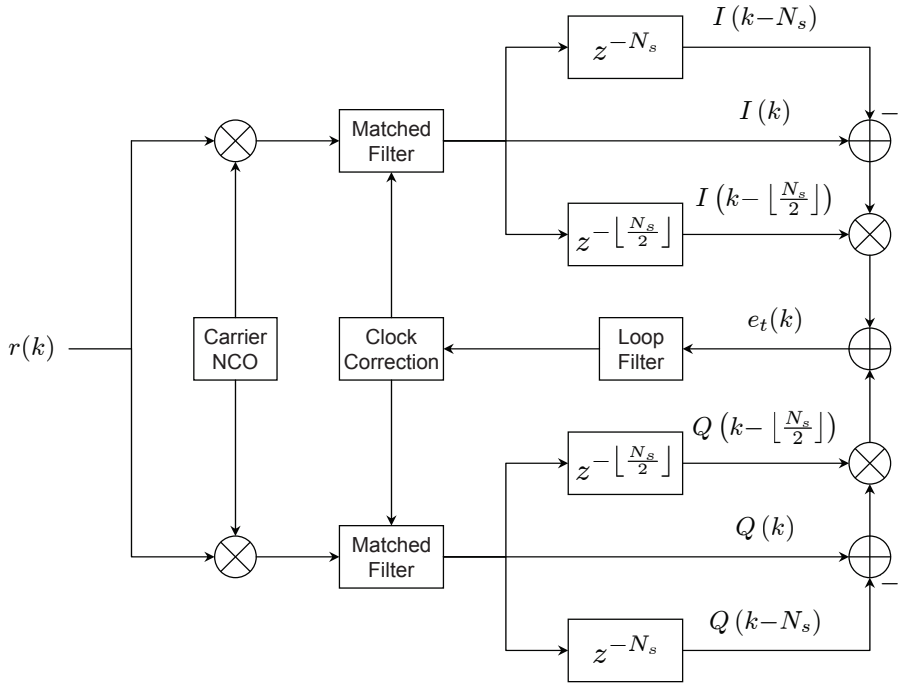

Figure 4. Gardner symbol synchronizer loop block diagram.

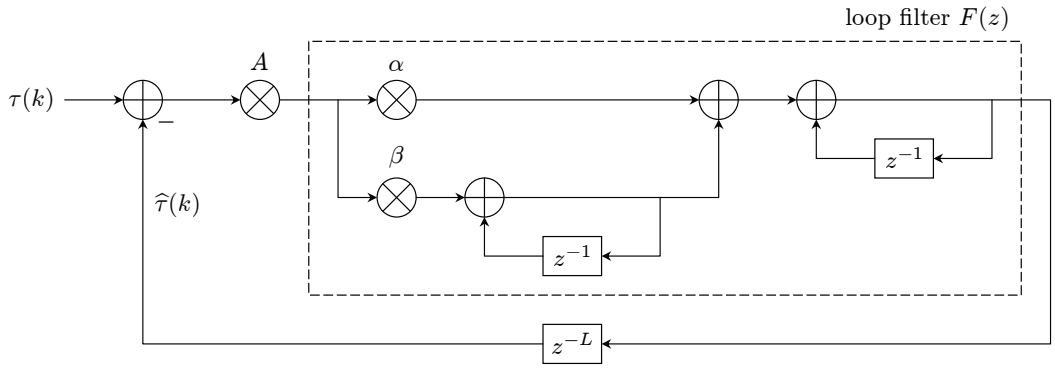

Figure 5. Baseband equivalent loop diagram.

numerically controlled oscillator (NCO) gain. In our implementation, $L = 1$ and $G_{nco} = 1$. The phase discriminator gain G_{pd} is obtained empirically by measuring the slope of the error characteristic curve, or S-curve, at zero timing error. The S-curve is a plot of the output of the error signal versus the input phase error. The noise-free S-curves for the DTTL and Gardner loops are given in Figures 6 and 7, respectively, for the case of 50 samples per symbol. Substituting Equation (2) into Equation (4), we can carry out the integration in Equation (3) numerically. From traditional phase-locked loop analysis [4], the filter coefficients α and β may be calculated for a second order loop with damping factor ζ and design loop bandwidth B_l^* as

$$\begin{aligned} \alpha &= \tfrac{1}{AK}\left(1 - e^{-2\zeta\omega_n T_u}\right) \\ \beta &= \tfrac{1}{AK}\left(1 + e^{-2\zeta\omega_n T_u} - 2e^{-\zeta\omega_n T_u}\cos(\omega_n T_u\sqrt{1-\zeta^2})\right) \end{aligned}$$

where the natural frequency ω_n is given by

$$\omega_n = 2\frac{B_l T_u}{\zeta T_u\left(1 + \frac{1}{4\zeta^2}\right)}$$

In order to evaluate the loop performance accurately, it must be calibrated to ensure that the implemented loop has damping factor and loop bandwidth as designed. This calibration consists of comparing the magnitude of the simulated loop transfer function with the theoretical loop transfer function. The simulated loop transfer function was obtained by calculating the ratio of the amplitude of output timing jitter to input timing jitter over a range of jitter frequencies. Figures 8 and 9 show the simulated transfer function along with the analytical expression. In addition, we show measured transfer functions for two hardware receivers tested at the Electronic Systems Test Laboratory (ESTL) at Johnson Space Center (JSC): the commercial T400XR receiver developed by RT Logic which we refer to hereinafter as the T400, and the Integrated Receiver (IR) developed at ESTL. In these cases the normalized design loop bandwidth was set to $B_l T_u = 0.001$, and an input timing jitter signal with TIE = 0.1 was used. The damping factors of $\zeta = 0.4$ and $\zeta = 13.9$ correspond to the values used in the T400 and IR receivers, respectively. Figure 8 shows good agreement between the analytical, simulated, and

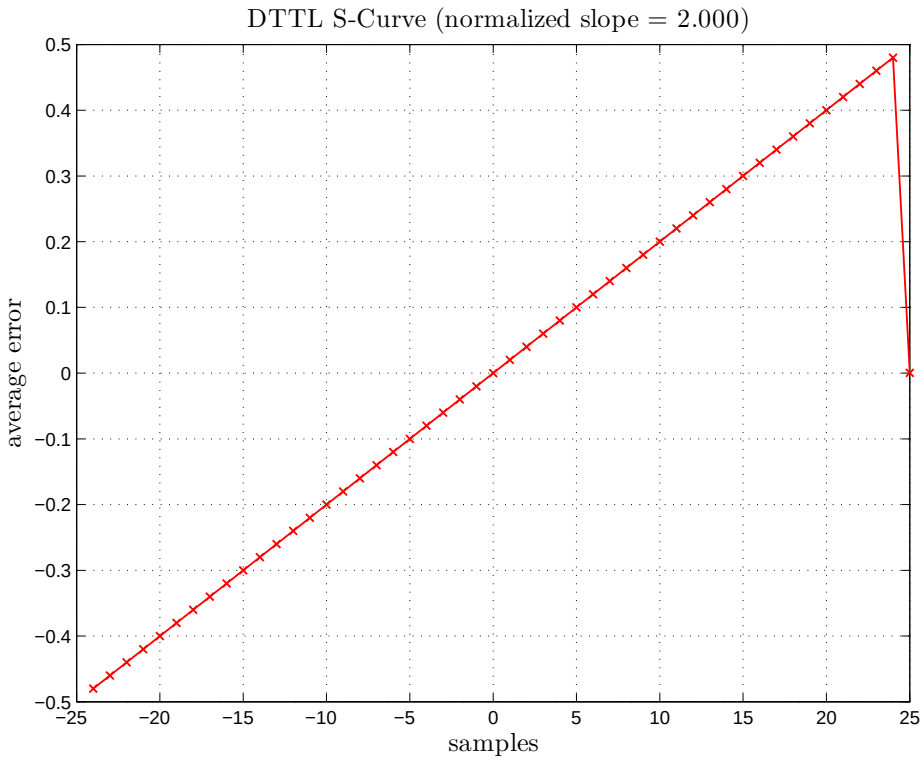

Figure 6. S-curve of data transition tracking loop.

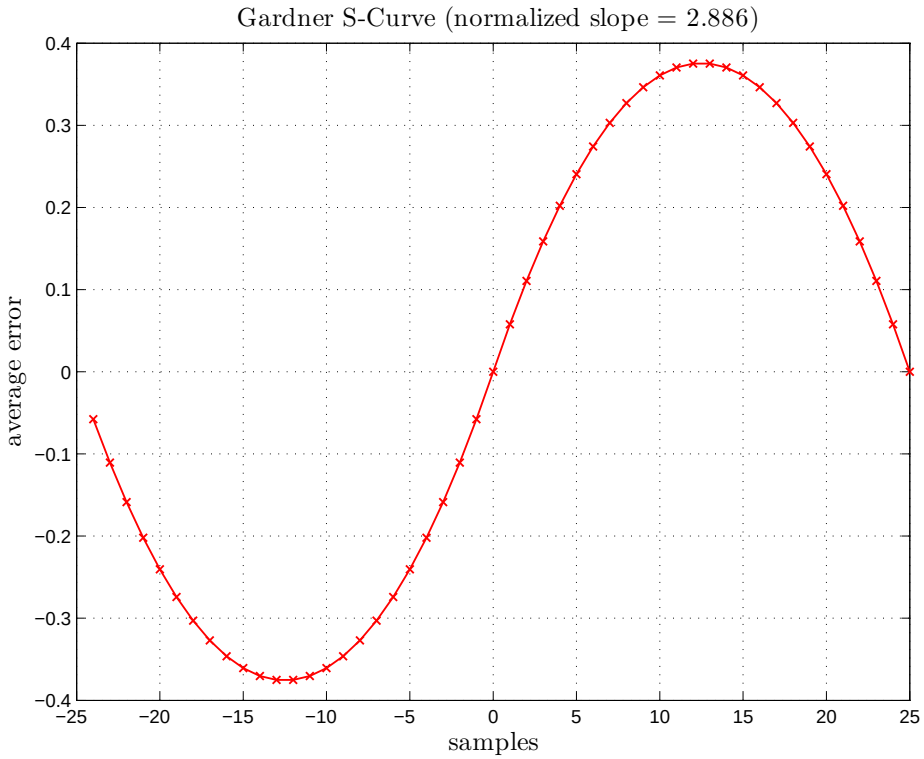

Figure 7. S-curve of Gardner tracking loop.

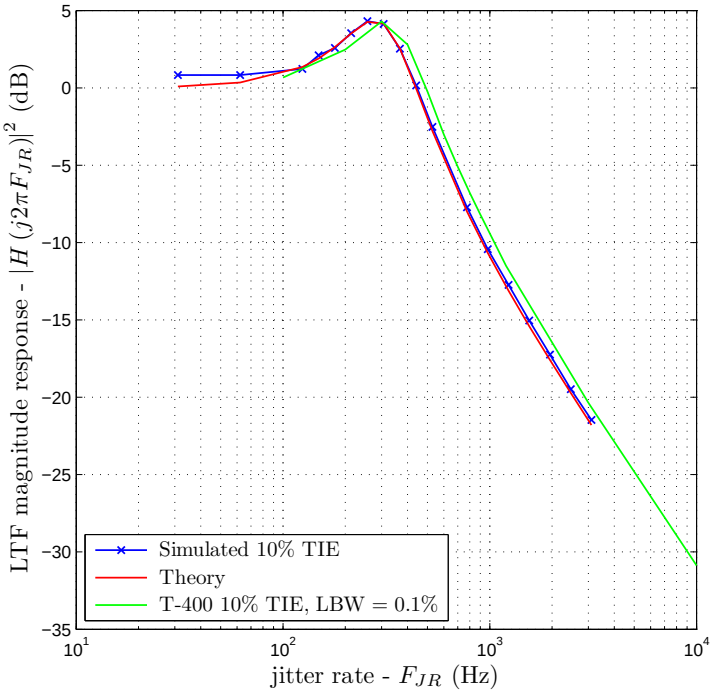

Figure 8. Analytical versus simulated Gardner loop transfer function for damping factor $\zeta = 0.4$, corresponding to the T400 commercial receiver.

hardware transfer functions, while Figure 9 shows that the simulated transfer function matches the analytical model well, but both are offset from the true measured hardware transfer function, indicating possibly flawed knowledge of the IR receiver loop parameters. However, the fact that the empirically derived transfer function matches the predicted analytical expression in both cases validates our loop modeling.

III. BER Degradation

A. Analysis

The effect of symbol timing errors upon the demodulated bit error rate may be calculated from

$$P(E) = \int_{-\frac{1}{2}}^{\frac{1}{2}} P(E \mid \lambda) f(\lambda)\, d\lambda \tag{5}$$

where $f(\lambda)$ is the probability density function (PDF) of the loop symbol timing error, and $P(E \mid \lambda)$ is the probability of bit error conditioned upon symbol timing error value λ. Assuming an NRZ pulse shape, $P(E \mid \lambda)$ is given by

$$P(E \mid \lambda) = \frac{1}{4}\text{erfc}(\sqrt{E_b/N_0}) + \frac{1}{4}\text{erfc}(\sqrt{E_b/N_0}(1 - 2|\lambda|))$$

where E_b/N_0 is the bit SNR. The symbol timing error at the output of the symbol synchronizer loop is modeled as the sum of two independent random variables: the loop output error due to thermal noise, and the loop output error due to residual sinusoidal

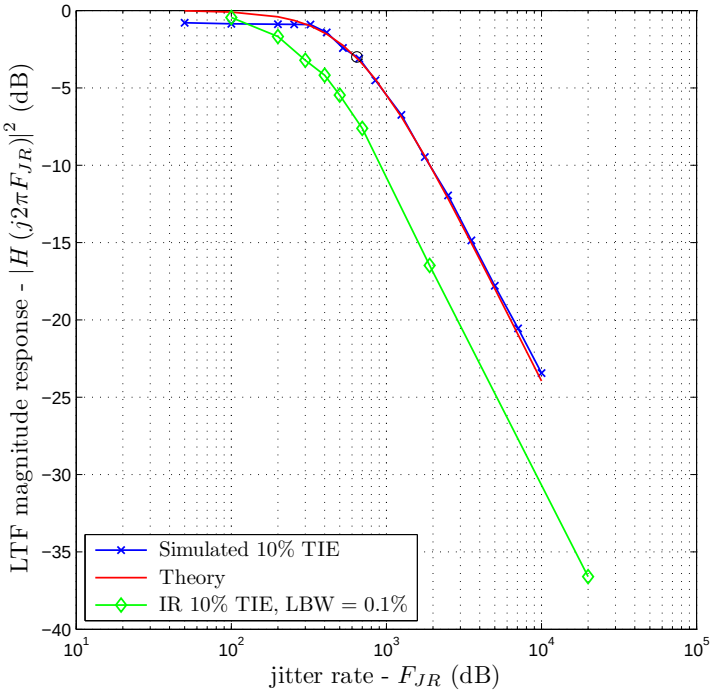

Figure 9. Analytical versus simulated Gardner loop transfer function for damping factor $\zeta = 13.9$, corresponding to the IR proprietary receiver.

jitter. Under this assumption of additive independent contributions to the timing error, its PDF is given by

$$f(\lambda) = f_N(\lambda) * f_S(\lambda) = \int_{-\infty}^{\infty} f_N(\mu) f_S(\lambda - \mu)\, d\mu \tag{6}$$

where $f_N(\lambda)$ is the PDF of the the thermal noise induced symbol timing error and $f_S(\lambda)$ is the PDF of the sinusoidal jitter induced symbol timing error. The PDF of the thermal noise induced symbol timing error $N(t)$ is modeled as Tikhonov, i.e.,

$$f_N(\lambda) = \frac{\exp(\rho_N \cos(2\pi\lambda))}{I_0(\rho_N)} \tag{7}$$

where $\rho_N = \frac{1}{(2\pi\sigma_N)^2}$ and σ_N^2 is the variance of the thermal noise symbol timing error. The PDF of the sinusoidal jitter induced symbol timing error $S(t)$ is given by [5]

$$f_S(\lambda) = \begin{cases} \frac{1}{\pi\sqrt{\sigma_S^2 - \lambda^2}}, & -\sigma_S < \lambda < \sigma_S \\ 0, & \text{otherwise} \end{cases} \tag{8}$$

where σ_S^2 is the variance of the sinusoidal jitter symbol timing error. Figure 10 illustrates the modeling of the symbol timing error. The validity of the assumption of additive independent contributions to symbol timing error was tested in a limited fashion by forming histograms of measured data from Block V Receiver hardware. Using a damping factor of $\zeta = 0.49$, normalized loop bandwidth $B_l T_u = 0.002$, input jitter TIE = 15.92%, and $\Delta F_{PJ} = F_{JR} = 0.001 R_d$, symbol timing error samples at the output of the DTTL were collected both in the noiseless case as well as at a bit SNR of 3 dB. Figure 11 shows

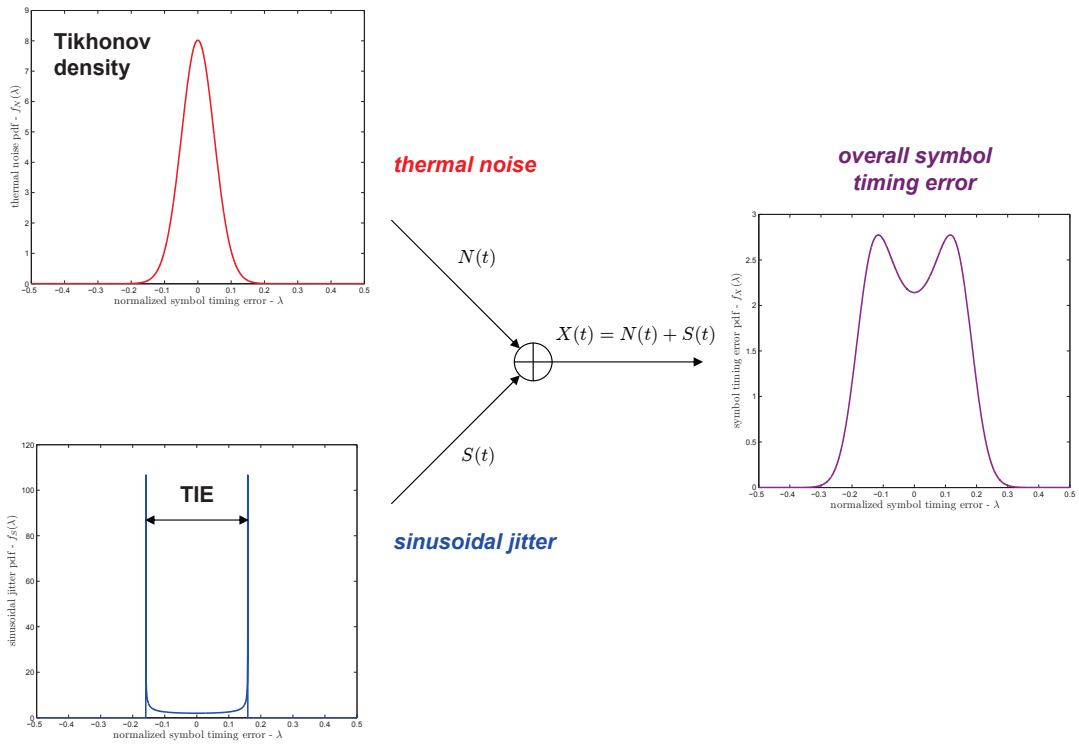

Figure 10. Additive model for symbol timing error.

these measured histograms, in addition to the analytical PDFs and simulated histograms. The noiseless data shows a measured TIE that is lower than the input TIE, but the functional form of the postulated symbol timing error pdf does appear to be consistent with both simulation and hardware results.

Using previously established results for the DTTL symbol synchronizer [6], the variance of the symbol timing error due to thermal noise is given by

$$\sigma_N^2 = \frac{\left(\frac{B_l}{R_d}\right)\xi\left(1+\frac{\xi E_b}{2N_0}-\frac{\xi}{2}\left[\frac{1}{\sqrt{\pi}}e^{-E_b/N_0}+\sqrt{E_b/N_0}\,\mathrm{erf}(\sqrt{E_b/N_0})\right]^2\right)}{2E_b/N_0\left[\mathrm{erf}(\sqrt{E_b/N_0})-\frac{\xi}{2}\sqrt{\frac{E_b}{\pi N_0}}e^{-E_b/N_0}\right]^2} \tag{9}$$

where ξ is the window length on the DTTL, B_l is the loop bandwidth, and R_d is the symbol rate. The variance of the sinusoidal jitter symbol timing error is given by [7]

$$\sigma_S^2 = \left(\frac{\Delta F_{PJ}}{2\pi F_{JR}}\right)^2 |G(j2\pi F_{JR})|^2 \tag{10}$$

where $G(s)$ is the jitter transfer function in the analog domain. The jitter transfer function is given by $G(s) = 1 - H(s)$, where $H(s)$ is the analog loop transfer function. Note that we use the analog analysis to predict performance, which is generally valid for $B_l T_u < 0.1$. The second order analog loop transfer function is given by

$$H(j2\pi F) = \frac{1 + j2\zeta\left(\frac{F}{F_n}\right)}{\left[1-\left(\frac{F}{F_n}\right)^2\right] + j2\zeta\left(\frac{F}{F_n}\right)} \tag{11}$$

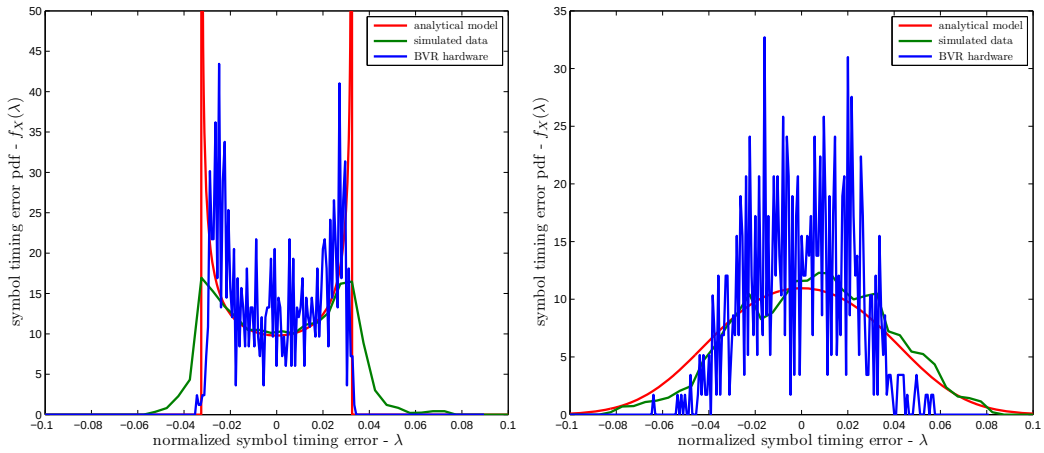

Figure 11. Histograms of Block V Receiver error signal samples at output of DTTL for (a) noiseless case, (b) $E_b/N_0 = 3$ dB.

where ζ is the loop damping factor and F_n is the natural frequency of the loop. F_n is related to the loop bandwidth and damping factor by

$$F_n = \frac{1}{\pi}\left(\frac{4\zeta}{4\zeta^2+1}\right)B_l \tag{12}$$

Equations (9) and (10) may be used in Equations (7) and (8), which in turn are used in Equations (6) and (5) to calculated resulting BER values. The actual BER degradation is then calculated as the additional bit SNR required to achieve a specified BER relative to required bit SNR in the absence of jitter. We see from Equations (9) and (10) that the contribution to symbol timing error from thermal noise depends upon the specific form of the symbol tracking loop, as well as loop bandwidth and SNR. On the other hand, the contribution to the symbol timing error from sinusoidal jitter is determined by the jitter parameters as well as the loop transfer function, which is dependent on the loop bandwidth and the loop damping factor. In Figure 12, we plot the BER degradation based upon the analytical expressions from Equations (5)-(10) as a function of the input jitter rate normalized to the loop bandwidth, for several damping factors. Here, TIE = 15.92%, corresponding to $\Delta F_{PJ} = F_{JR}$, and the normalized loop bandwidth was set to $B_l T_u = 0.001$. The degradation was measured at a BER of 0.1, corresponding to a nominal bit SNR of $E_b/N_0 = -0.856$ dB. We see that at the lowest damping factor of $\zeta = 0.2$, the degradation peaks to over 4 dB at a jitter rate of $0.22B_l$, which is the natural frequency of the loop at $\zeta = 0.2$, from Equation (12). Similarly, when $\zeta = 0.4$, the BER degradation peaks at a jitter rate near the corresponding loop's natural frequency, but with a much lower value of about 1.25 dB. As the damping factor increases, the peak degradation value decreases, but in all cases, the degradation at jitter rates beyond the loop bandwidth converges to the same asymptotic value regardless of damping factor.

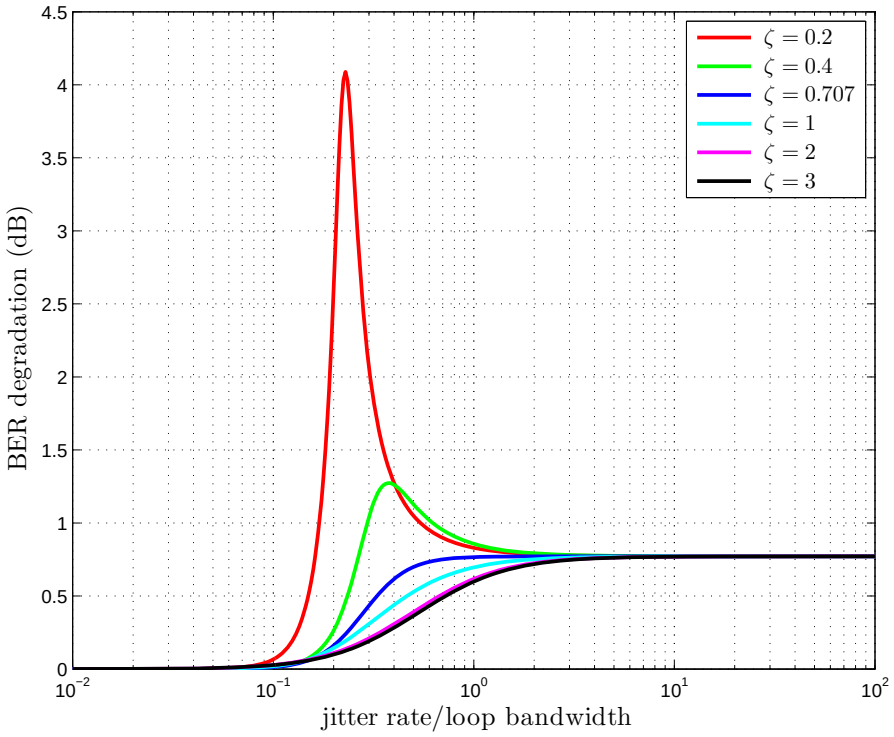

Figure 12. BER degradation versus normalized jitter rate for several values of damping factor ζ.

B. Simulation Results

Monte Carlo simulations of the system shown in Figure 1 were performed in Matlab in order to test specific tracking loop implementations and compare BER degradation results with the analytically predicted values, as well as with previously measured hardware results. Initial simulations showed that both the M-DTTL and Gardner loops performed comparably, while the single-armed conventional DTTL performed slightly worse. We therefore performed subsequent BER degradation simulations for the M-DTTL and Gardner loops using varying TIE values and the two damping factors $\zeta = 0.4$ and $\zeta = 13.9$. Results are shown in Figure 13 for a 2 Mbps OQPSK signal sampled at 50 samples per symbol, with $B_l T_u = 0.001$, for the underdamped loop corresponding to the T400 receiver with $\zeta = 0.4$. From the plots in Figure 13, we observed that in all cases the peak degradation occurs near the natural frequency of the transfer function, and that it is larger for the M-DTTL than for the Gardner loop. As the TIE value increases, the degradation increases, and at TIE = 15.92%, cycle slips occurred at jitter rate near the loop's natural frequency. In all cases, the general trends of the hardware measurements, simulations, and analytically predicted values are similar, but while the asymptotic BER degradation values are approximately the same for analysis and simulation, the measured hardware BER degradation is lower asymptotically. In the loop's tracking region ($F_{JR}/B_l < 1$), the analytical degradation is slightly lower than the simulation values.

In Figure 14, we show the analogous results for the overdamped loop with $\zeta = 13.9$,

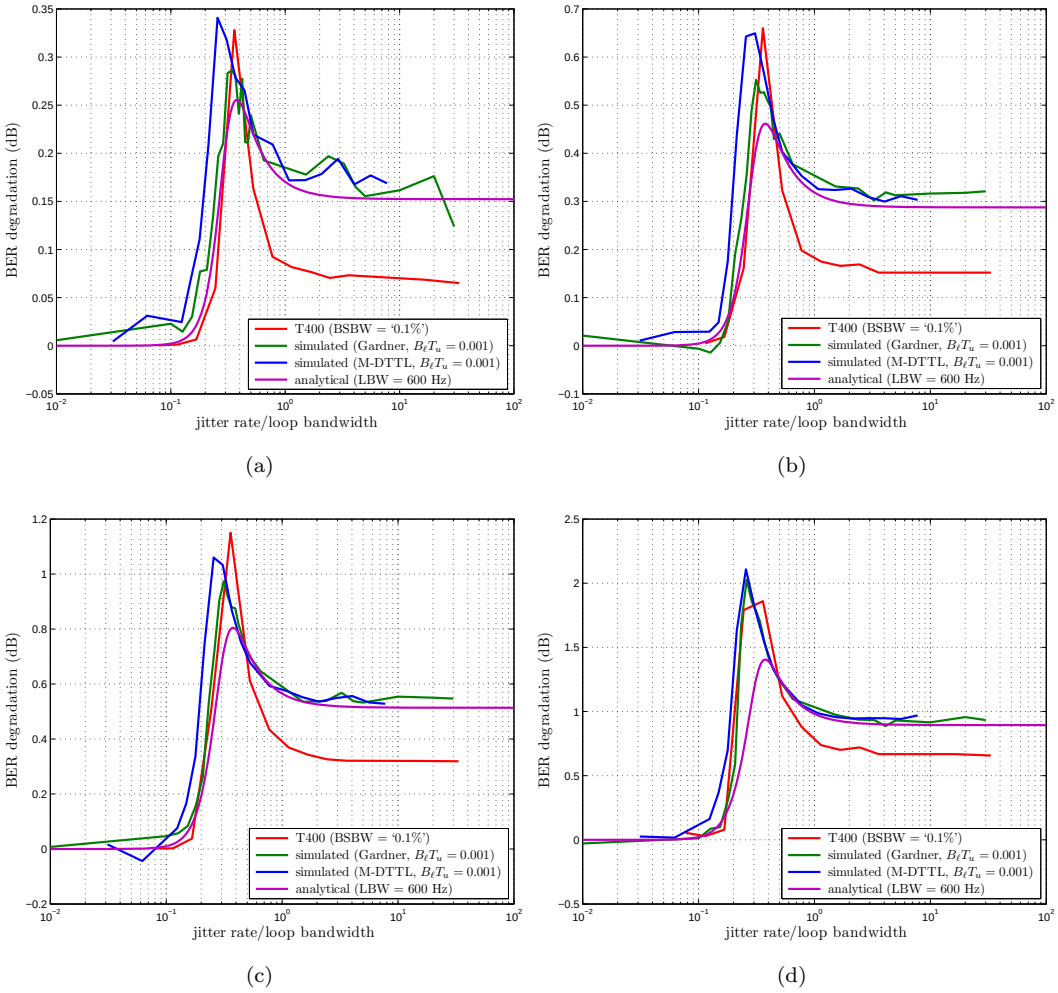

Figure 13. Degradation versus normalized jitter rate at 0.1 BER with underdamped loop ($\zeta = 0.4$), for TIE values of (a) 5.03%**, (b)** 7.39%**, (c)** 10.84%**, and (d)** 15.92%**.**

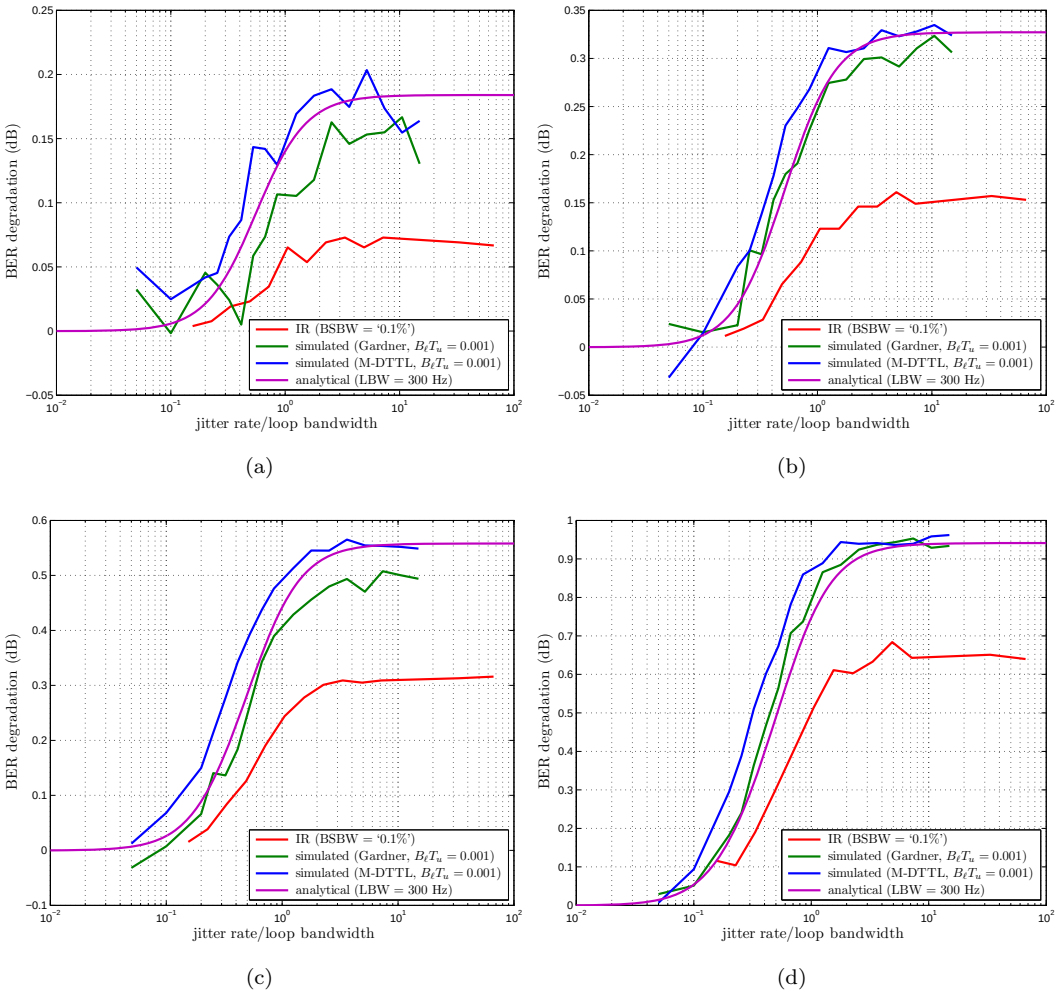

Figure 14. Degradation versus normalized jitter rate at 0.1 BER with overdamped loop ($\zeta = 13.9$), for TIE values of (a) 5.03%**, (b)** 7.39%**, (c)** 10.84%**, and (d)** 15.92%**.**

corresponding to the IR. We note that while the asymptotic degradation values are the same here as in the underdamped case, there is no peak at the natural frequency of the loop, and the increased damping factor results in lower degradation in the loop's tracking region. We also observe that the M-DTTL consistently incurs slightly more degradation than the Gardner loop, and that again, the asymptotic degradation for the analysis and simulation is higher than for the hardware measurements. The reason for this discrepancy in the untracked region is not known.

Figure 15 shows BER degradation results when the jitter rate is much larger than the loop bandwidth. Simulated degradation results for both the Gardner loop and M-DTTL are shown as a function of TIE, for several values of loop bandwidth, in addition to analytically predicted degradation values and measured hardware results. We see again from this plot that the degradation caused by untracked jitter is not a function of the loop damping factor, and that for both the analytical curves as well as for the simulated ones,

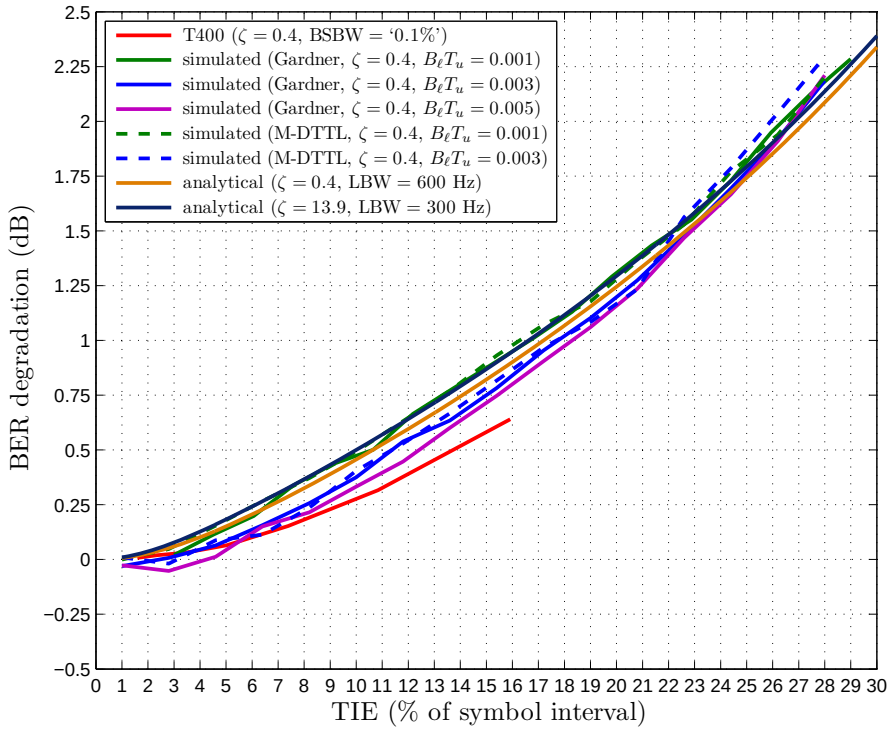

Figure 15. BER degradation versus TIE in the untracked jitter region.

the degradation increases as the loop bandwidth decreases. We attribute this dependence on loop bandwidth to the larger role of sinusoial jitter relative to that of the thermal noise at narrower loop bandwidths.

Figures 16 and 17 show surface plots with BER degradation plotted versus peak jitter and jitter rate, both of which are normalized to the symbol rate. These plots are generated strictly from the analytical formulas, and define the regions of peak jitter and jitter rate that result in less than a specified level of degradation. Figure 16 assumes a damping factor of 0.4 and 600 Hz loop bandwidth, while Figure 17 uses a damping factor of 13.9 and 300 Hz loop bandwidth. Superimposed on the plots is the SNUG multiple access (MA) and S-band single access (SSA) (MA/SSA) return mask [2] that specifies allowable transmit jitter levels. Note that the unevaluated regions in the plot correspond to TIE values greater than one symbol duration. We see from these figures that if the requirement is to have less than 1 dB of BER degradation, the SNUG mask is insufficient at the parameters tested here. The degradation surface has a "V" shape in the underdamped case, while in the overdamped case the surface shape is more of a "U", partly cut off in the given jitter rate range. The slopes of the sides of the "V" may be defined as particular values of TIE on the positive slope side, and as values of CCJ on the negative slope slide. We may therefore analytically derive requirements on the transmit jitter in terms of TIE and CCJ given a maximum allowable BER degradation value, an observation that has been made previously by [1].

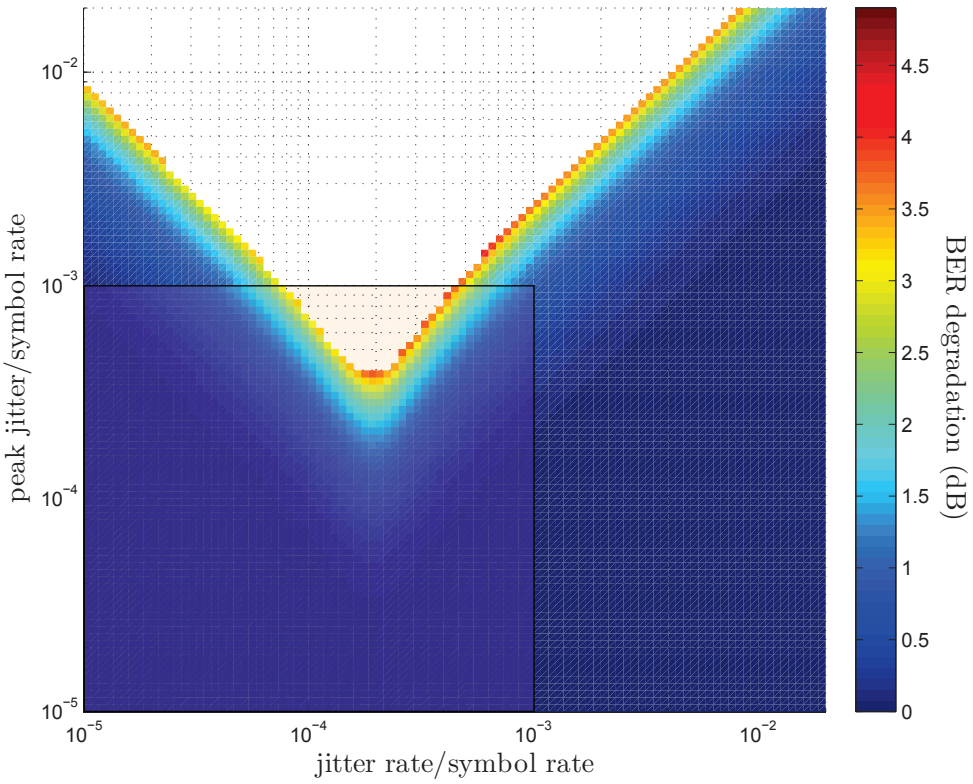

Figure 16. BER degradation surface plot as a function of peak jitter and jitter rate for $\zeta = 0.4$.

C. BER Degradation for Multi-tone Jitter

The question that naturally arises when considering these results is whether the single-tone sinusoidal transmit symbol jitter model is realistic. While limited testing of flight hardware has validated this model to a certain extent, it is also of interest to consider how a multi-tone model of jitter affects BER degradation results. Towards that end, simulations were run in which two additional tones offset in frequency by $\pm f_0 = 0.001R_d$ from the primary jitter component were added to the model. BER degradation curves as a function of normalized jitter rate are shown in Figure 18 for four different TIE values. For each plot, the simulated M-DTTL degradation results in the presence of the multi-tone sinusoidal jitter are shown for three damping factors: $\zeta = 0.4$, $\zeta = 1.0$, and $\zeta = 13.9$, and the results are compared with the measured hardware results for the T400 and IR receivers under the single-tone jitter conditions. These results show that as the frequency content is spread over multiple tones, the peak degradation is significantly lower than in the single tone case, and that the degradation is highest for the underdamped loop ($\zeta = 0.4$). Extrapolating this effect, we would expect that wideband jitter would result in even lower peak degradation, provided that the total energy remained constant.

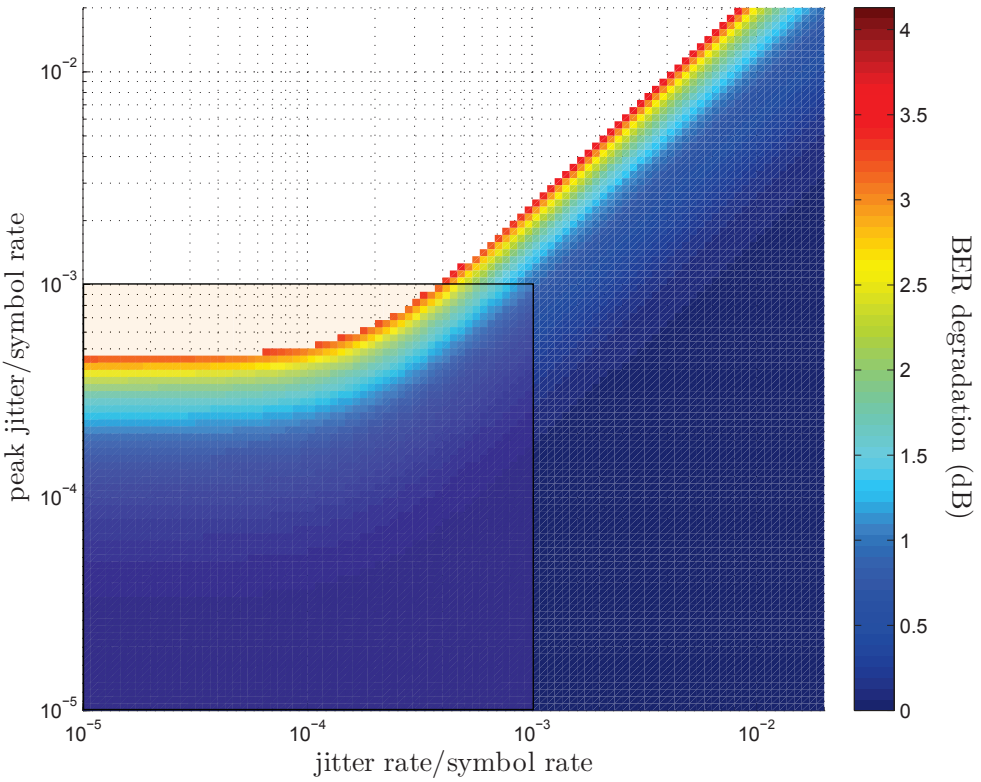

Figure 17. BER degradation surface plot as a function of peak jitter and jitter rate for $\zeta = 13.9$.

IV. Cycle Slip Probability

In addition to BER degradation, transmit symbol jitter may also cause cycle slipping, which refers to the phenomena of the receiver symbol clock phase changing by 360°, or one cycle. Cycle slipping causes entire symbols to be dropped from the data stream, which can then cause entire codeword frames to be in error. Thus, requirements on cycle slip probability are typically strict, on the order of 10^{-10} or less [8]. Specifications on transmit symbol jitter must therefore ensure low probability of cycle slip in addition to a certain tolerable level of BER degradation.

Figure 19 shows an example of the error signal output from the symbol synchronizer loop. We can see areas of steady state tracking where the error signal is flat, while cycle slips are denoted by "x" marks, showing where the error signal has changed by more than a symbol. The cycle slip rate may be calculated by counting the number of these events. Note that there are times in which many cycle slips occur consecutively – these are counted as a single event unless there is a period of at least 2000 symbols, or approximately one codeword frame, between them.

Unlike the BER degradation, the cycle slip probability in the presence of sinusoidal symbol timing jitter is difficult to evaluate analytically. However, there are analytical expressions for the cycle slip rate when only thermal noise is present, assuming a second order DTTL

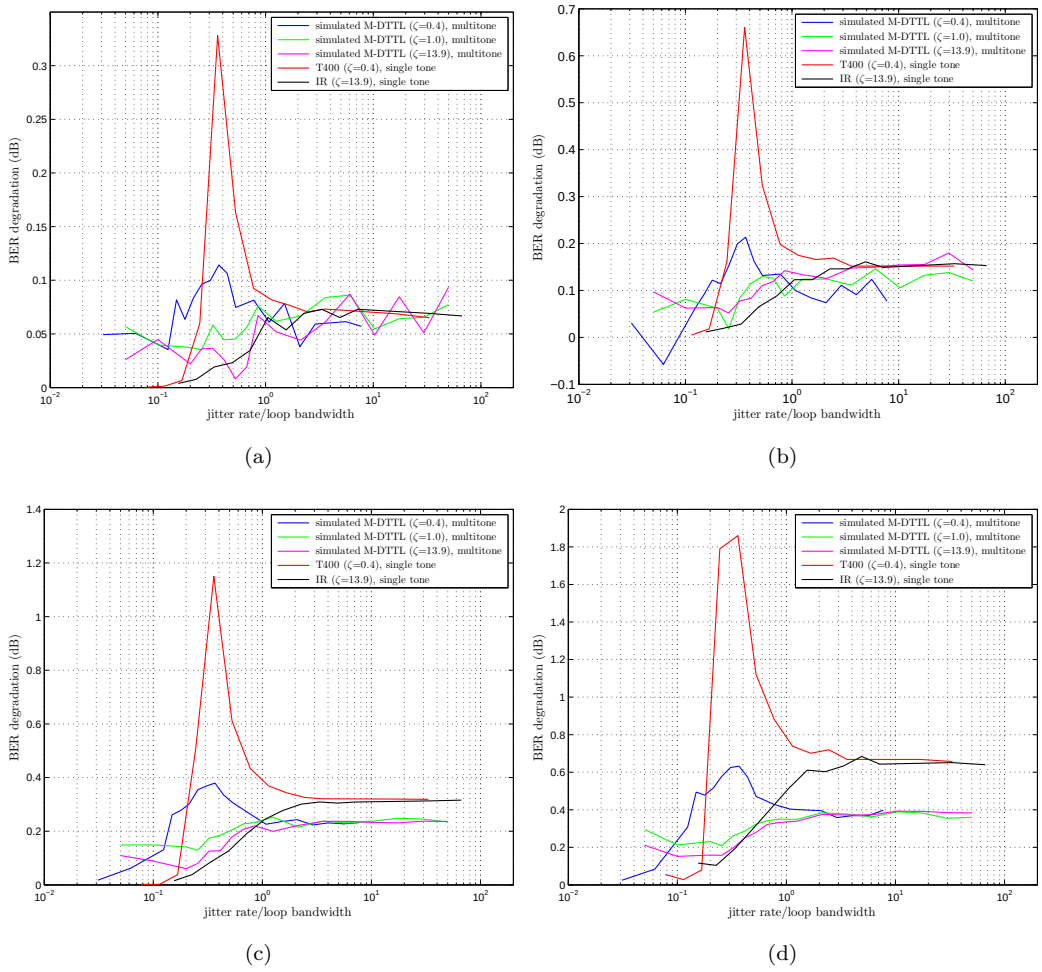

Figure 18. Degradation versus normalized jitter rate at 0.1 BER with three sinusoidal jitter components, using simulation of M-DTTL, for TIE values of (a) 5.03%**, (b)** 7.39%**, (c)** 10.84%**, and (d)** 15.92%**.**

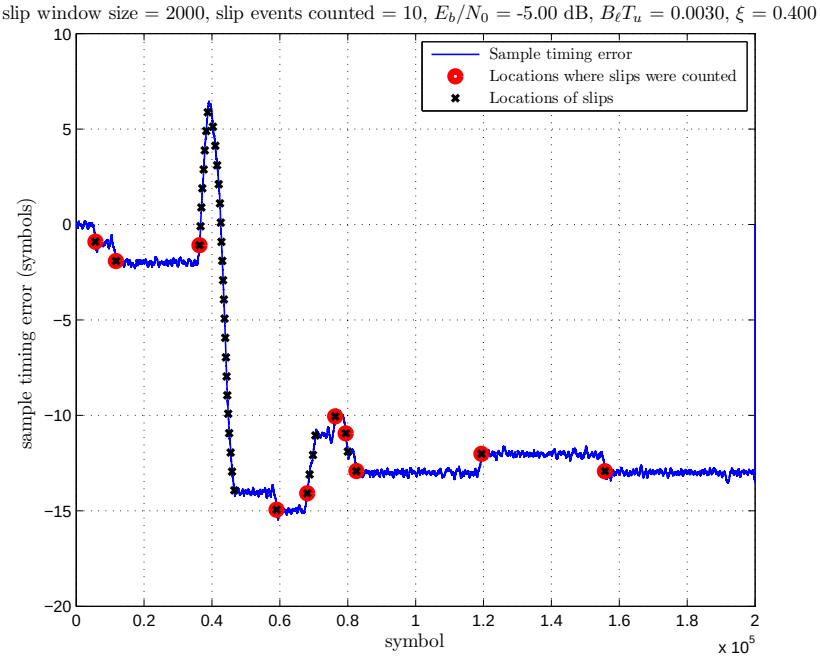

Figure 19. Symbol synchronizer output error signal showing cycle slip events.

[9]. The cycle slip rate is given by

$$S = \frac{1}{R_b T_{slip}} \tag{13}$$

where R_b is the bit rate and T_{slip} is the mean time between slip events. T_{slip} may be calculated numerically as

$$T_{slip} = \int_0^1 \left[\exp\left(-\int_0^x a(z)\,dz\right)\right]\left\{\int_0^x b(w)\left[\exp\left(\int_0^w a(z)\,dz\right)\right]\right\}dx$$

where

$$a(x) = -\left(\frac{r+1}{r}\right)\frac{\rho}{g_n'(0)}g_n(x) + \left(\frac{\rho}{r g_n'(0)}\right)x \tag{14}$$

and

$$b(x) = \left(\frac{r+1}{r}\right)^2 \frac{\rho}{2B_l g_n'(0)} \tag{15}$$

Here, $r = 4\zeta^2$, where ζ is the loop damping factor, ρ is the loop SNR, B_l is the loop bandwidth, and $g_n(\lambda)$ is the normalized S-curve for the DTTL, given by

$$g_n(\lambda) = \begin{cases} \lambda\,\mathrm{erf}\left(\sqrt{\frac{E_b}{N_0}}(1-2\lambda)\right) - \frac{1}{8}(\xi-2\lambda)\left[\mathrm{erf}\left(\sqrt{\frac{E_b}{N_0}}\right) - \mathrm{erf}\left(\sqrt{\frac{E_b}{N_0}}(1-2\lambda)\right)\right], & 0 \le \lambda \le \frac{\xi}{2} \\ \frac{\xi}{2}\,\mathrm{erf}\left(\sqrt{\frac{E_b}{N_0}}(1-2\lambda)\right), & \frac{\xi}{2} \le \lambda \le \frac{1}{2} \end{cases}$$

The parameter ξ is the DTTL window length. The slope of the normalized DTTL S-curve is given by

$$g_n'(0) = \mathrm{erf}(\sqrt{E_b/N_0}) - \frac{\xi}{2}\sqrt{\frac{E_b/N_0}{\pi}}e^{-E_b/N_0} \tag{16}$$

These expressions may be used to place lower bounds on the cycle slip probability in the presence of jitter.

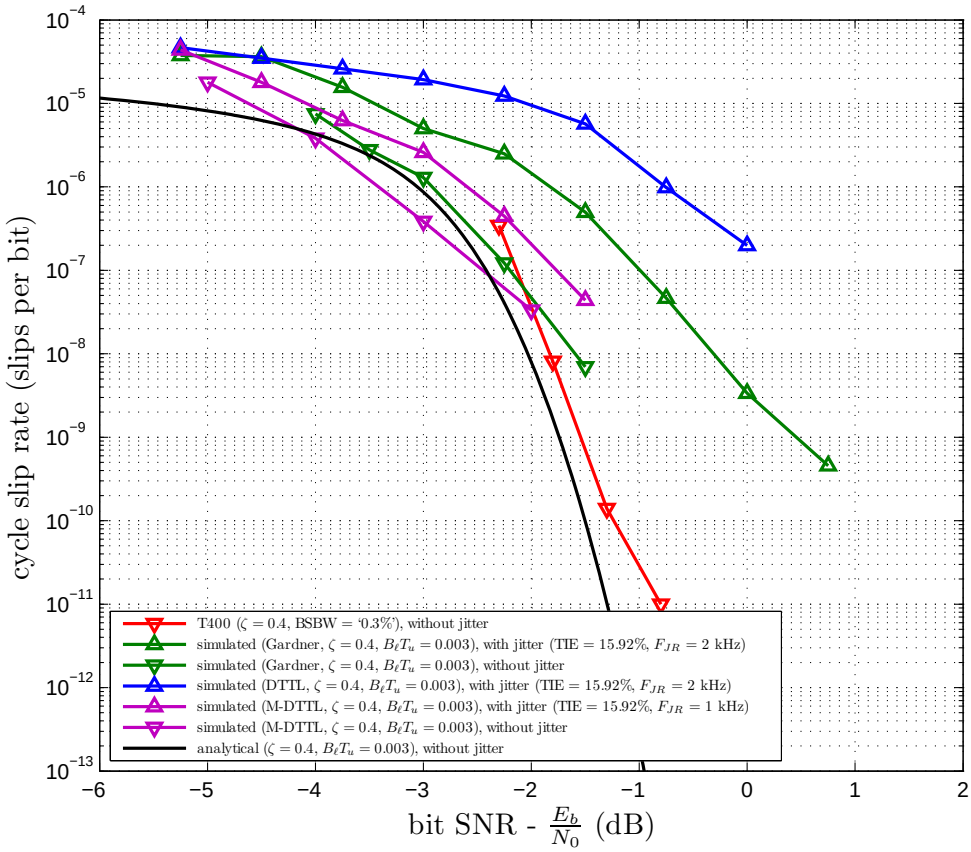

Figure 20. Cycle slip probabilities for 2 Mbps OQPSK for DTTL, M-DTTL, and Gardner symbol synchronizers with $B_l T_u = 0.003$ and $\zeta = 0.4$.

Figures 20 and 21 show cycle slip rates obtained from our Matlab Monte Carlo simulation, along with the analytical lower bound obtained from Equations (13)-(16), as well as measured slip rates from the T400 hardware in the absence of jitter. Figure 20 shows the cycle slip rate in slips per bit as a function of bit SNR for the DTTL, M-DTTL, and Gardner symbol synchronizers, all using a normalized loop bandwidth of $B_l T_u = 0.003$ and an underdamped loop with $\zeta = 0.4$ (corresponding to the T400 damping factor). Again, 2 Mbps OQPSK was considered, and the TIE of the sinusoidal jitter was set to 15.92%, while the jitter rate was set to either 1 kHz or 2 kHz. The DTTL performed significantly worse in the presence of jitter than the M-DTTL or Gardner loops. In the absence of jitter, the T400 hardware and the simulated Gardner results track the analytical curve well, while the M-DTTL simulation performed slightly better at points. Clearly, for the jitter parameters tested here, cycle slip rates are significantly degraded in the presence of jitter, with larger degradation for the 2 kHz jitter rate than for the 1 kHz jitter rate.

Figure 21 shows an augmented set of cycle slip probabilities, now showing results using an overdamped loop with $\zeta = 5$. We see that increasing the damping factor reduces the cycle slip probability significantly, with the analytical curves in the absence of jitter shifting to the left by over 7 dB at a 10^{-12} cycle slip rate. We note that the 10^{-12} target bit slip rate

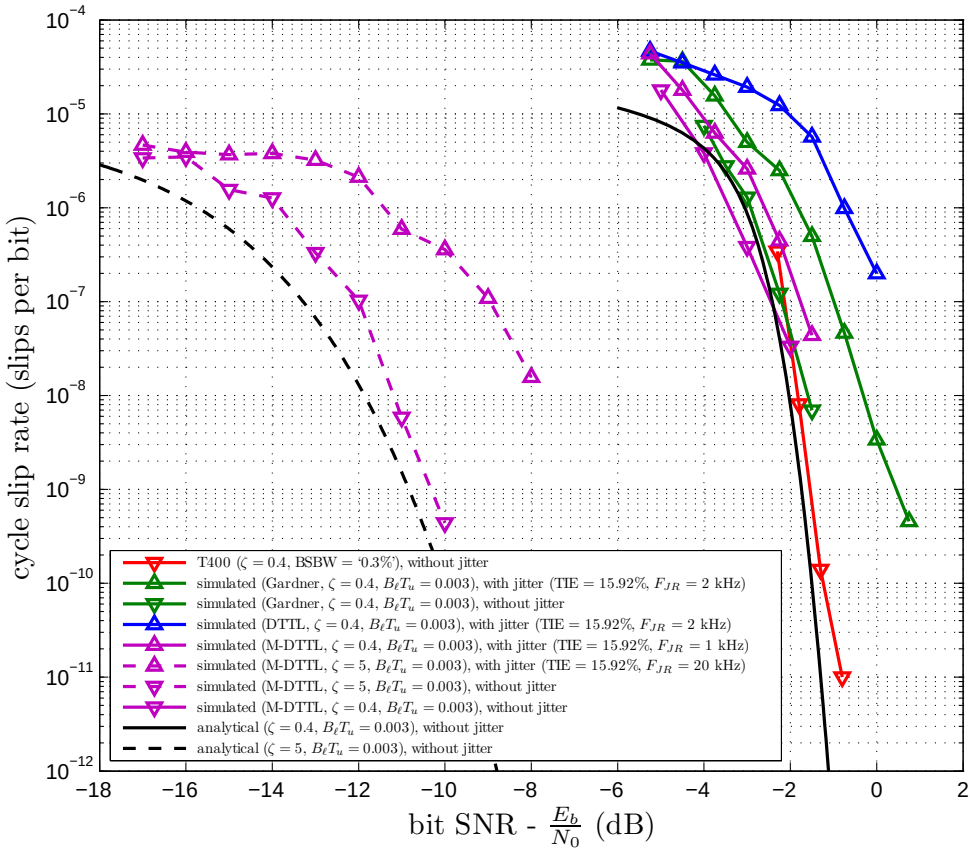

Figure 21. Cycle slip probabilities for 2 Mbps OQPSK for DTTL, M-DTTL, and Gardner symbol synchronizers with $B_l T_u = 0.003$, and with both $\zeta = 0.4$ and $\zeta = 5$.

at $E_b/N_0 = -0.83$ dB looks like it can be met by using the higher damping factor of $\zeta = 5$ at a TIE of 15.92% and jitter rate of 20 kHz, which is outside the tracking region of the $B_l T_u = 0.003$ loop. Although the IR receiver has an even higher damping factor of 13.9, the cycle slip rate simulations took prohibitively long at this parameter.

V. Conclusions

In this article we documented the effect of transmitter clock jitter upon receiver symbol synchronization performance assuming a sinusoidal model for the timing jitter. The BER degradation was derived both analytically and via a Monte Carlo simulation for uncoded OQPSK with ideal rectangular NRZ pulses. It was shown that peak degradation decreases as the loop damping factor increases, and that for underdamped tracking loops, the BER degradation peaks when the normalized jitter rate is approximately the same as the natural frequency of the loop transfer function. While there was some discrepancy between measured hardware BER degradation and analytical values outside the loop's tracking region, for unknown reasons, it was shown that peak degradation could be estimated well using analytical expressions, providing us with an important tool in predicting

performance in the presence of transmit symbol jitter. Simulated cycle-slip rates were also presented, showing that proper selection of the loop damping factor can mitigate the catastrophic impact of transmit symbol clock jitter upon cycle slip probabilities.

Acknowledgments

The authors would like to thank Chatwin Lansdowne from the NASA Johnson Space Center in Houston, Texas, for providing valuable and extensive hardware test data as well as insightful comments on the subject of sinusoidal symbol jitter. In addition, special thanks go out to Michael Cheng from the Information Processing Group at JPL for helping the authors interface with Chatwin Lansdowne. Last, but not least, the authors would like to thank Dennis Lee from the Signal Processing Research Group at JPL for contributing hardware results from the Block V Receiver in addition to providing valuable feedback on the subject of timing jitter.

References

[1] C. Lansdowne, A. Schlesinger, D. Lee, and M. Cheng, "Jitter Induced Symbol Slip Rates in Next-Generation Ground Segment Receivers," in *Proceedings of 2010 AIAA SpaceOps Conference*, Huntsville, Alabama, April 2010.

[2] *Space Network Users' Guide*, Revision 9 ed., NASA Goddard Space Flight Center, August 2007.

[3] U. Mengali and A. N. D'Andrea, *Synchronization Techniques for Digital Receivers*. New York: Plenum Press, 1997.

[4] W. C. Lindsey and C. M. Chie, "A Survey of Digital Phase-Locked Loops," *Proceedings of the IEEE*, vol. 69, no. 4, pp. 410–431, April 1981.

[5] C. M. Chie and C.-S. Tsang, "The Effects of Transmitter/Receiver Clock Time-Base Instability on Coherent Communication System Performance," *IEEE Transactions on Communications*, vol. COM-30, no. 3, pp. 510–515, March 1982.

[6] M. K. Simon, S. M. Hinedi, and W. C. Lindsey, *Digital Communication Techniques*. Englewood Cliffs, New Jersey: Prentice Hall, 1995.

[7] C.-S. Tsang and C. M. Chie, "Effect of Signal Transition Variation on Bit Synchronizer Performance," *IEEE Transactions on Communications*, vol. 41, no. 5, pp. 673–677, May 1993.

[8] *Space Network User Service Subsystem Replacement Systems Requirement Document*, NASA Goddard Space Flight Center, June 2009.

[9] R. Tausworthe, "Cycle Slipping in Phase-Locked Loops," *IEEE Transactions on Communication Technology*, vol. COM-15, no. 3, pp. 417–421, June 1967.